Dual Link Image Coding Based on CCSDS-123

Joan Bartrina-Rapesta and Francesc Aulí-Llinàs, *Senior Member, IEEE*

***Abstract*—Predictive coding techniques are attractive for image codecs because they can yield high compression efficiency while spending few computational resources. In remote sensing, predictive techniques are employed in prominent standards to transmit images captured by Earth Observation (EO) satellites. Although EO satellites have full duplex capacity, compression standards for spatial data are devised to use the downlink only. Recently, we presented a dual link image coding system that employs both the uplink and the downlink to accelerate the transmission of such images. The proposed system was introduced in the wavelet-based JPEG2000 standard, which is not well-suited for satellites due to its complexity. This paper approaches the dual link scheme to a more suitable standard for spatial data based on predictive coding, more precisely, the Lossless Multispectral and Hyperspectral image compression standard CCSDS-123.0-B.2. The proposed method adapts the dual link image coding scheme to CCSDS-123.0-B-2 by incorporating a quantizer, a lightweight arithmetic coder, and a rate control technique. Experimental results suggest that the resulting system achieves higher coding ratios than CCSDS-123.0-B-2 and JPEG2000 with dual link.**

***Index Terms*—Dual link image coding, CCSDS-123.0-B-2, remote sensing images.**

I. Introduction

Earth Observation (EO) satellites are of prominent interest in many fields due to their large variety of applications for the management of natural resources, monitoring of natural disasters and climate change, or emergency planning, among others. In general, EO satellites revolve around the Earth from the North to the South Pole at an altitude between 100 to 10,000 miles. Although these satellites commonly have full duplex capacity, meaning that their communication link can upload and download data simultaneously while in contact with the ground station, the harvested data are transmitted employing only the downlink. Ground stations are, in general, situated at either pole because these areas have the longest transmission windows. These windows only last a few minutes, so compression techniques that increase coding efficiency allow the transmission of (more) images with higher quality.

There is a great interest in the image compression field to explore different coding techniques to download image data from EO satellites. An inherent difference among techniques comes from the use of transform or predictive coding. Transform-based coding systems [1]–[12] employ a transform, such as the discrete wavelet transform, that produces a lesser redundant transformed image that is entropy coded. Predictive-based coding systems [13]–[20] employ a predictor that estimates the image samples using the already processed data. The predictor reduces the image redundancy, producing the so-called residuals that are entropy coded. In general, prediction techniques require fewer computational resources than transform-based schemes. Regardless of using transform or predictive coding, compression schemes can offer lossless, near-lossless or lossy regimes. Images transmitted with lossless [5], [9], [11], [13]–[15], [20] and near-lossless [2], [3], [5], [12], [14], [16], [20] compression are identical to those captured by the satellite, or with some pre-determined maximum distortion. Lossy compression [1], [2], [4], [7], [8], [17]–[19] achieves higher compression ratios at the expense of quality losses.

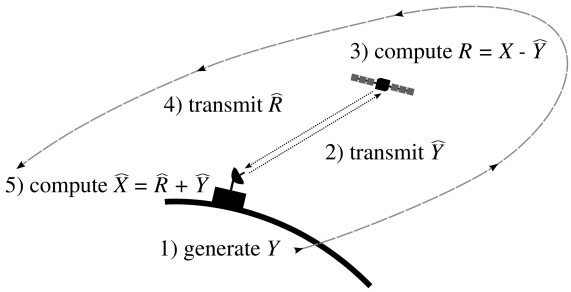

Fig. 1: Overview of the dual link image coding scheme.

The polar orbit of EO satellites results in the acquisition of a different ground area (from pole to pole) at each orbit due to the Earth's rotation. Most satellites use a sun-synchronous orbit, which places them at the same area at the same time of the day after a pre-determined number of orbits. This is called the repeat cycle. The images acquired in each repeat cycle are very similar or, in other words, they have high temporal redundancy except for meteorological events and changes in the vegetation or ground. Traditionally, this redundancy has not been exploited to increase the compression efficiency of coding systems in satellites. Recently, we introduced a dual link image coding scheme [10] that uses both the temporal redundancy and the full duplex capacity of satellites. The main idea, illustrated in Fig. 1, is to use already-stored data of the satellite to generate a reference image, denoted by Y, on the ground. The compressed representation of Y is denoted by $\widehat{Y}$, which is transmitted to the satellite via the uplink. The satellite uses both $\widehat{Y}$ and the acquired image X to compute the residual $R = X - \widehat{Y}$. R is compressed on the satellite resulting in $\widehat{R}$, which is transmitted to the ground via the downlink. The ground station then recovers the captured image as $\widehat{X} = \widehat{R} - \widehat{Y}$.

The system that we proposed in [10] employs the JPEG2000 standard (ISO/IEC 15444). JPEG2000 is a widespread transform-based coder. It achieves excellent coding performance and provides advanced features such as scalability by quality, resolution, and spatial position. Its coding system

This work was supported in part by the Spanish Ministry of Science, Innovation and Universities (MICIU) and by the European Regional Development Fund (FEDER) under Grant RTI2018-095287-B-I00, and by the Catalan Government under Grant 2017SGR-463. J. Bartrina-Rapesta and F. Aulí-Llinàs are with the Department of Information and Communications Engineering, Universitat Autònoma de Barcelona, E-08193 Bellaterra, Barcelona, Spain (e-mail: joan.bartrina@uab.cat).

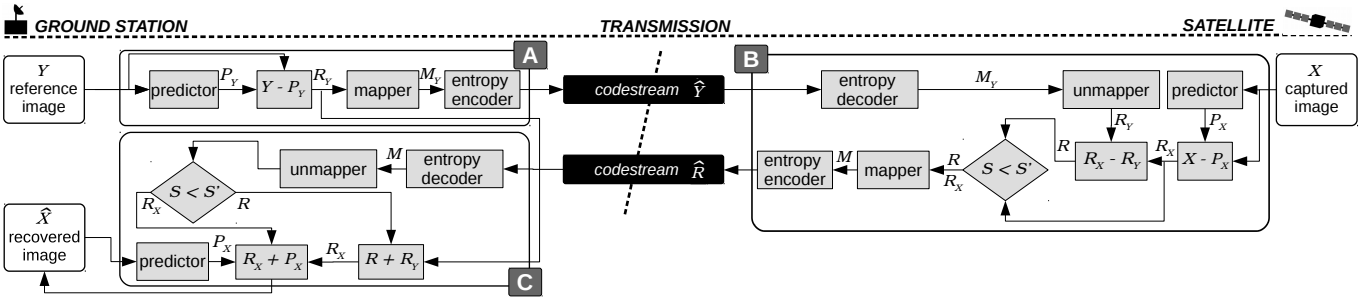

Fig. 2: Illustration of the coding pipelines of the three modules of CCSDS-123-DLIC.

is mainly devised for conventional hardware architectures, requiring abundant computational resources. To the best of our knowledge, JPEG2000 is not employed in EO satellites. Satellites have limited resources, so compression standards for spatial image data are devised to suit the computational architectures available in space. The Consultative Committee for Space Data Systems (CCSDS) [21] is the principal organization responsible for proposing coding systems tailored for spatial environments. In 2019, CCSDS published its latest standard, the CCSDS-123.0-B-2 [22] (CCSDS-123 onward), focused on predictive lossless compression for multispectral and hyperspectral images.

This work introduces the dual link image coding scheme in CCSDS-123. The main difference between JPEG2000 and CCSDS-123 is that the former is transform-based, whereas the latter uses low-complexity predictive techniques. In JPEG2000, the dual link scheme computes the residuals in the wavelet domain. Herein, the system is adapted to CCSDS-123 by computing the residuals in the predictive stage of the coder. Additionally, a quantizer, rate control technique, and lightweight arithmetic coder are added to allow the use of the full duplex capacity of the satellite and offer lossy compression. The proposed method achieves higher compression ratios than those of CCSDS-123 and JPEG2000 with dual link.

The rest of the paper is structured as follows. Section II introduces the dual link image coding scheme in the framework of CCSDS-123 and Section III presents experimental results. The last section concludes with a summary.

II. CCSDS-123 WITH DUAL LINK

The system proposed herein is based on both our previous dual link image coding scheme for JPEG2000 [10] and our improvement of the CCSDS-123 standard presented in [20]. The coding pipeline of CCSDS-123 has three main coding stages: prediction, mapping, and entropy coding. The codec in [20] uses the original predictor and mapper of CCSDS-123, substitutes the entropy coder by a lightweight contextual arithmetic coder, and introduces a quantizer. It is named CCSDS-123-AC. Such modifications allow the codec to operate in lossy compression regimes.

As seen in Fig. 2, the CCSDS-123-AC with dual link image coding (CCSDS-123-DLIC) has three modules: A) an encoder at the ground station that compresses the reference image, B) a decoder and encoder at the satellite that decompresses the reference image, decorrelates the redundancy between the reference and the captured image, and compresses the resulting data, and C) a decoder at the ground station that decompresses the received data and generates the recovered image.

Module A in CCSDS-123-DLIC (upper-left corner in Fig. 2) codes the reference image Y that is transmitted to the satellite. This codec employs the coding pipeline of [20], which is similar to that of the CCSDS-123. First, a predictor estimates the image samples, denoted by P_Y, employing already coded data. The residuals, computed as $R_Y = Y - P_Y$, are mapped to a non-integer value M_Y that is fed to the entropy coder. The output of the entropy coder is the codestream denoted by $\widehat{Y}$, which is transmitted to the satellite. As described below, both Module A and Module B may employ a quantizer and rate control technique (not shown in Fig. 2) for lossy compression.

Module B (right corner in Fig. 2) has the image captured by the satellite, referred to as X, and receives $\widehat{Y}$ from the ground station via the uplink. This codec first recovers R_Y applying the inverse entropy coder and mapper, and computes $R_X = X - P_X$, with P_X denoting the estimate of X obtained from the conventional predictor of CCSDS-123. R_Y and R_X are the residuals respectively obtained from the reference and captured image. Since both utilize the same predictor, they can be decorrelated to obtain $R = R_X - R_Y$. This step exploits the temporal redundancy of the images captured by the satellite, embodied in R_Y, to achieve higher compression efficiency. Note that, differently from Fig. 1, this operation is applied in the prediction domain to avoid decoding the original image. Even so, these operations increase the computational complexity of this module about 60% with respect to a conventional coding scheme.

As described in [10], the use of temporal redundancy benefits compression when *no* meteorological or other events veil the ground. When such events occur, the coding scheme must disregard the temporal information (i.e., R_Y) to avoid losing coding efficiency. This is applied selectively depending on the spatial area of the image. The natural form to do so is to use the spatial partitions that are employed by the codec to code the data, so that the features of the coding system are practically unaffected. CCSDS-123 codes the data in a line-by-line fashion, so the proposed technique carries out this selective coding using (segments of) lines. Similarly as in [10], the absolute sum of the residuals R and R_X is employed. More precisely, $S = \sum_i R_i$ and $S' = \sum_i R_{X_i}$, with R_i and R_{X_i} respectively denoting the residuals of R_X and R_Y, and the residuals of X within the segment. If $S < S'$, then the system feds R_i to the next stage of the coding pipeline as depicted in Fig. 2. Otherwise, it disregards the

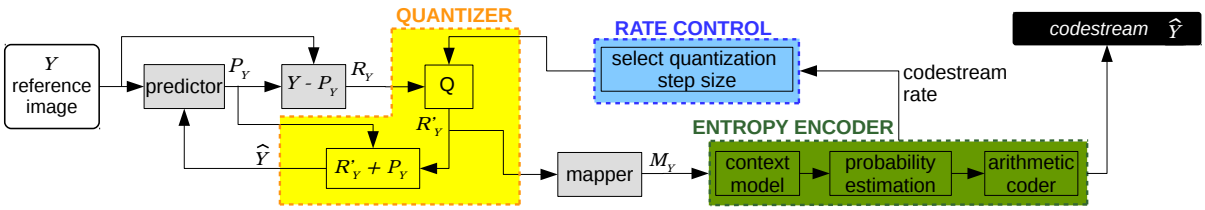

Fig. 3: Illustration of Module A of CCSDS-123-DLIC with the proposed modifications highlighted in: yellow for the quantizer, blue for the rate control, and green for the lightweight contextual arithmetic coder.

temporal redundancy and uses R_{X_i}. This is a computationally inexpensive operation that is repeated in each segment line. Auxiliary information indicating this coding decision is sent with each segment's data. The length of the segment affects compression efficiency due to the granularity achieved to identify veiled areas and due to the use of more or less auxiliary information. Section III evaluates this aspect with experimental tests. The final stages in Module B are the mapper, which generates M, and the entropy coder, which outputs the codestream $\widehat{R}$ that is transmitted to the ground station.

Module C (lower-left corner in Fig. 2) recovers the satellite image employing codestream $\widehat{R}$ and residuals R_Y, which were previously computed in Module A. First, the codestream is entropy decoded and M is unmapped to R. The auxiliary information embedded in the codestream signals whether each line-segment were coded with residuals R_i or R_{X_i}. If R_i were used, then $R_X = R + R_Y$. The recovered image is obtained via $\widehat{X} = R_X + P_X$. When lossless compression is used, the recovered image is equal to that captured by the satellite (i.e., $\widehat{X} = X$), otherwise $\widehat{X}$ may contain some distortion.

The compression regime is aided in our codec by a rate control method that regulates the amount of distortion introduced by the quantization of the residuals. Fig. 3 depicts the operations that are carried out in Module A when rate control is needed to offer lossy compression. Equivalent operations are introduced in Module B. Module C also incorporates a dequantizer when lossy regimes are used (rate control is not needed in this module). The modifications with respect to a conventional CCSDS-123 coder are highlighted in Fig. 3. The quantizer is emphasized in yellow. In our codec, the quantizer controls the maximum error that the residuals R_Y may attain, denoted by R'_Y. Since the predictor at the decoder only has R'_Y available, the encoder must also use R'_Y when predicting the image samples. This is depicted in Fig. 3 through the feedback line between the quantizer and the predictor. This feedback provides $Y' = R'_Y - P_Y$ so that Y' is employed to generate P_Y for the following samples, as the decoder does. This technique is also used in other works for similar purposes [17], [23]. The rate control allows the quantizer to introduce more or less distortion depending on the target rate for the final codestream. The technique employed herein is based on [19], which enables lossy and near-lossless regimes at the expense of slightly penalizing coding efficiency. It assigns different quantization step sizes to the data segments depending on the statistics of the image.

The entropy coder of the original CCSDS-123 is replaced by the lightweight contextual arithmetic coder proposed in [20]. Briefly explained, this arithmetic coder employs the already coded data of the neighbors of the current residual to select a context. The context is associated with a probability, which is employed by the arithmetic coder to achieve compression. The probability of each context is adaptively adjusted as more residuals are coded. In Module A, this coder is applied as in [20], employing M_Y to form the context. The entropy coder in Modules B and C is applied after deciding whether the segment is coded with or without the reference image (via the condition $S < S'$). If the reference image is used, the context in the entropy coder is selected employing M_Y in addition to M since our experience indicates that this slightly improves compression efficiency. Otherwise, the context is selected employing M only.

III. Experimental Results

The corpus of [10] is used in the following tests. This corpus has two temporal series that were harvested by the Landsat 8 satellite during a period of a year, generating a collection of 45 images and more than 15 GB of data. All images in both series have a resolution of 4096×4096, 11 components, and a bit-depth of 16 bits per sample (bps). The series are named "Barcelona" and "Salt Lake City" referring to the Earth areas that were acquired. More details and the complete image series can be found in [10]. An important aspect of the dual link image coding scheme is the generation of the reference image Y. Three strategies are evaluated in [10]. The strategy that yields the highest coding performance uses the immediately previous acquired image of the same area. This strategy is also used in the following tests. Instead of using the original CCSDS-123, CCSDS-123-AC is employed in the following to provide a fair comparison with CCSDS-123-DLIC (since the same arithmetic coder and rate control technique are employed in both systems). The parameters of the CCSDS-123-AC predictor are selected leaning on results of [24] as those that achieve the highest coding efficiency as follows: full mode sum type, neighbor oriented predictor mode, prediction bands set to 3, and adaptation rate set to 3.

The first test analyses the impact of the segment length on the coding efficiency. Three representative images of the "Barcelona" temporal series (with acquisition dates 8/3/15, 12/6/14, and 4/29/15) are employed. These images are selected to assess the proposed method in different conditions. They have high, medium, and low correlation with the reference

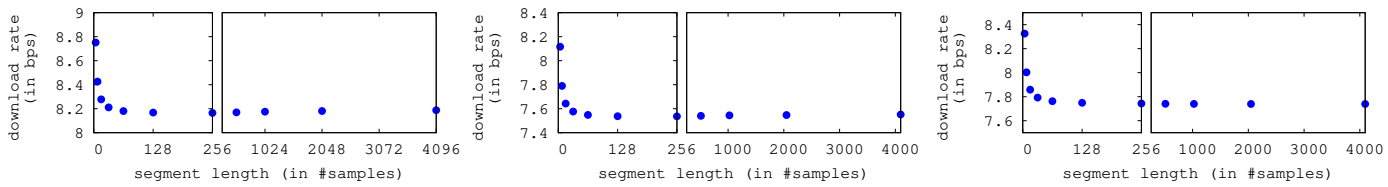

(a) "Barcelona" 8/3/15 (high correlation) (b) "Barcelona" 12/6/14 (medium correlation) (c) "Barcelona" 4/29/15 (low correlation)

Fig. 4: Evaluation of lossless coding performance for CCSDS-123-DLIC when using different segment lengths.

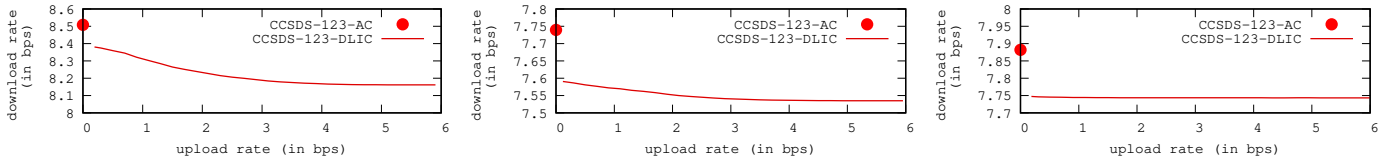

(a) "Barcelona" 8/3/15 (high correlation) (b) "Barcelona" 12/6/14 (medium correlation) (c) "Barcelona" 4/29/15 (low correlation)

Fig. 5: Evaluation of lossless coding performance for CCSDS-123-DLIC depending on the upload rate.

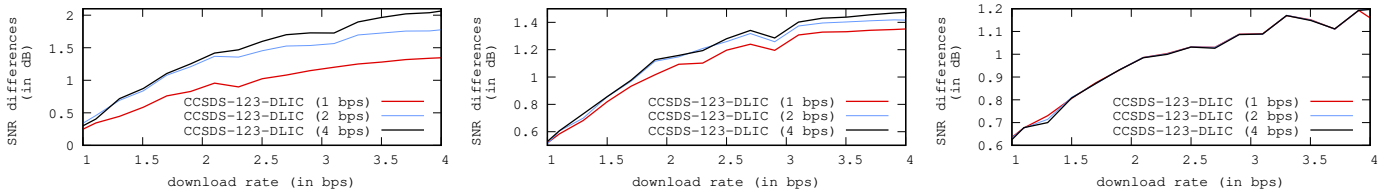

(a) "Barcelona" 8/3/15 (high correlation) (b) "Barcelona" 12/6/14 (medium correlation) (c) "Barcelona" 4/29/15 (low correlation)

Fig. 6: Evaluation of lossy coding performance for CCSDS-123-DLIC with three different upload rates. Results are reported as the difference between CCSDS-123-DLIC and CCSDS-123-AC.

image Y, mostly due to meteorological events. Fig. 4 (a), (b) and (c) depict in the vertical axis the download rate (or the minimum channel capacity of the downlink) needed to transmit the images with a lossless regime when different segments lengths are employed. In this test, all codecs employ a lossless regime. As seen in the figure, short segments penalize the coding efficiency due to the coding of auxiliary information. Segments of approximately 256 samples or more yield the highest compression efficiency, so they are used in the remaining tests. These results also hold for lossy regimes.

The next test assesses lossless coding performance when the ground station transmits the reference image Y in lossy mode at different rates. Fig. 5 depicts the achieved results. The vertical axis is the download rate to losslessly transmit the image, whereas the horizontal axis is the rate of the uploaded codestream $\widehat{Y}$ (or the minimum channel capacity of the uplink). The figure also depicts the lossless rate achieved by CCSDS-123-AC. We recall that these modes can only be used for lossless compression. These results suggest that CCSDS-123-DLIC can improve the coding performance in approximately from 0.1 to 0.3 bps with respect to CCSDS-123-AC. The maximum gains are achieved for "Barcelona" 8/3/15 when the uplink transmits 4 bps or more. Lower rates for $\widehat{Y}$ yield lower gains since the reference image has more distortion. The benefits achieved with the other two images are inferior due to lower correlation between X and Y. Results for JPEG2000 are not reported in this and the following test for illustration purposes, since the performance of JPEG2000 is approximately 1 bps above that reported in these tests (see Fig. 7 in [10]).

The third test evaluates the lossy coding performance achieved by the proposed method with respect to that of CCSDS-123-AC. The vertical axis of Fig. 6 depicts the Signal to Noise Ratio (SNR) difference between CCSDS-123-DLIC and CSSDS-123-AC when the satellite downloads the codestream $\widehat{R}$ at different rates. The figure reports the results when the codestream $\widehat{Y}$ is uploaded with a rate of 1, 2, and 4 bps. These results indicate that CCSDS-123-DLIC obtains a recovered image of higher quality than that achieved by CCSDS-123-AC, with gains of almost 2 dB in Fig. 6(a) when both $\widehat{R}$ and $\widehat{Y}$ are transmitted at 4 bps. Again, the gains are higher as higher is the correlation with the reference image. When Y is poorly correlated with X, increasing the upload rate does not help to enhance the image quality. This is seen in Fig. 6(c) as the three plots achieving the same performance.

The last test evaluates the lossless coding performance achieved on average for all images of the two temporal series for JPEG2000, JPEG2000-DLIC, CCSDS-123, CCSDS-123-AC and CCSDS-123-DLIC. In [10] JPEG2000 does not exploit the spectral redundancy due to its computatioal demand, thus and for comparison purposes, the results reported for CCSDS-123-AC include two different configurations for the prediction bands, more precisely, when 0 (P=0) and 3 (P=3) bands are employed. In addition, results for CCSDS-123 for Integer (IC) and Block Adaptive (BC) are provided for P=3. Table I reports the achieved results. CCSDS-123-DLIC attains the lowest coding rate for both temporal series. Results also indicate that CCSDS-123-AC largely benefits

TABLE I: Evaluation of the lossless coding performance for all images of each temporal series. The results report the download rate expressed in bps.

	upload rate (in bps):	0.1	0.5	1	2	4
Barcelona	JPEG2000	9.21				
	JPEG2000-DLIC	9.02	8.98	8.93	8.87	8.82
	CCSDS-123 (IC)	8.26				
	CCSDS-123 (BC)	8.36				
	CCSDS-123-AC (P=0)	9.11				
	CCSDS-123-AC (P=3)	8.26				
	CCSDS-123-DLIC	**8.20**	**8.19**	**8.17**	**8.15**	**8.12**
Salt Lake City	JPEG2000	8.99				
	JPEG2000-DLIC	8.81	8.87	8.75	8.70	8.67
	CCSDS-123 (IC)	8.20				
	CCSDS-123 (BC)	8.27				
	CCSDS-123-AC (P=0)	8.92				
	CCSDS-123-AC (P=3)	8.20				
	CCSDS-123-DLIC	**8.17**	**8.16**	**8.15**	**8.12**	**8.10**

from the use of 3 prediction bands. When none prediction band is used, the coding rates achieved by CCSDS-123-AC are very similar to those of JPEG2000 since JPEG2000 neither exploits redundancies among bands. JPEG2000-DLIC obtains slightly lower rates than JPEG2000 and CCSDS-123-AC (P = 0) though they are significantly higher than those of CCSDS-123-AC (P = 3) and CCSDS-123-DLIC. Finally, CCSDS-123-DLIC outperforms CCSDS-123 for both scenes, again increasing the upload rate of the CCSDS-123-DLIC enhances the benefits of CCSDS-123-DLIC.

IV. Conclusions

We recently introduced a dual link image coding system based on JPEG2000 that has shown that the use of the full duplex capacity of EO satellites may improve the compression performance when coding imagery harvested by such satellites. This paper introduces the dual link image coding scheme to the CCSDS-123 standard, which is more tailored for the spatial environment. The main idea is to predict a reference image on the ground, which is employed by the satellite to increase the coding efficiency of the compression system. Differently to JPEG2000, CCSDS-123 is based on prediction coding, so the adoption of the dual link scheme requires in-depth modifications in the coding pipeline. Experimental results suggest that the proposed method achieves higher coding efficiency, both in lossless and lossy regimes, than CCSDS-123 based techniques and JPEG2000. Coding gains depend on the correlation between the reference and captured image, and on the available upload rate. Although current satellites have uplinks with a low channel capacity, future missions may consider its expansion to enable the use of the proposed, or other similar, dual link coding techniques.

References

[1] B. Penna, T. Tillo, E. Magli, and G. Olmo, "Progressive 3-D coding of hyperspectral images based on JPEG 2000," *IEEE Geoscience and Remote Sensing Letters*, vol. 3, no. 1, pp. 125–129, Jan. 2006.

[2] G. Carvajal, B. Penna, and E. Magli, "Unified Lossy and Near-Lossless Hyperspectral Image Compression Based on JPEG 2000," *IEEE Geoscience and Remote Sensing Letters*, vol. 5, no. 4, pp. 593–597, Oct. 2008.

[3] C. W. Chen, T. C. Lin, S. H. Chen, and T. K. Truong, "A Near Lossless Wavelet-Based Compression Scheme for Satellite Images," in *2009 WRI World Congress on Computer Science and Information Engineering*, vol. 6, Mar. 2009, pp. 528–532.

[4] F. Auli-Llinas, M. W. Marcellin, J. Serra-Sagrista, and J. Bartrina-Rapesta, "Lossy-to-Lossless 3D Image Coding through Prior Coefficient Lookup Tables," *ELSEVIER Information Sciences*, vol. 239, no. 1, pp. 266–282, Aug. 2013.

[5] I. Blanes, E. Magli, and J. Serra-Sagrista, "A Tutorial on Image Compression for Optical Space Imaging Systems," *IEEE Geoscience and Remote Sensing Magazine*, vol. 2, no. 3, pp. 8–26, Sep. 2014.

[6] Q. Du, N. Ly, and J. E. Fowler, "An Operational Approach to PCA+JPEG2000 Compression of Hyperspectral Imagery," *IEEE Journal of Selected Topics in Applied Earth Observations and Remote Sensing*, vol. 7, no. 6, pp. 2237–2245, Jun. 2014.

[7] J. Bartrina-Rapesta, F. Auli-Llinas, I. Blanes, and J. S. Sagrista, "Cell-Based 2-Step Scalar Deadzone Quantization for JPEG2000," in *IEEE Proceedings of Data Compression Conference*, Mar. 2014, pp. 143–152.

[8] J. Beerten, I. Blanes, and J. Serra-Sagrista, "A Fully Embedded Two-Stage Coder for Hyperspectral Near-Lossless Compression," *IEEE Geoscience and Remote Sensing Letters*, vol. 12, pp. 1775–1779, Aug. 2015.

[9] N. Amrani, J. Serra-Sagrista, V. Laparra, M. W. Marcellin, and J. Malo, "Regression Wavelet Analysis for Lossless Coding of Remote-Sensing Data," *IEEE Transactions on Geoscience and Remote Sensing*, vol. 54, no. 9, pp. 5616–5627, Sep. 2016.

[10] F. Auli-Llinas, M. Marcellin, V. Sanchez, J. Bartrina-Rapesta, and M. Hernandez-Cabronero, "Dual Link Image Coding for Earth Observation Satellites," *IEEE Transactions on Geoscience and Remote Sensing*, vol. 56, no. 9, pp. 5083–5096, Sep. 2018.

[11] S. Alvarez-Cortes, J. Bartrina-Rapesta, and J. Serra-Sagrista, "Multilevel Split Regression Wavelet Analysis for Lossless Compression of Remote Sensing Data," *IEEE Geoscience and Remote Sensing Letters*, vol. 15, no. 10, pp. 1540–1544, Oct. 2018.

[12] S. Alvarez-Cortes, J. Bartrina-Rapesta, M. Marcellin, and J. Serra-Sagrista, "Regression Wavelet Analysis for Near-lossless Remote Sensing Data Compression," *IEEE Transactions on Geoscience and Remote Sensing*, vol. 58, no. 2, pp. 790–798, Oct. 2019.

[13] ISO/IEC, "JPEG-LS lossless and near-lossless compression for continuous-tone still images," 1999.

[14] E. Magli, G. Olmo, and E. Quacchio, "Optimized Onboard Lossless and Near-Lossless Compression of Hyperspectral Data Using CALIC," *IEEE Geoscience and Remote Sensing Letters*, vol. 1, no. 1, pp. 21–25, Jan. 2004.

[15] F. Rizzo, C. Bruno, G. Motta, and J. A. Storer, "Low-Complexity Lossless Compression of Hyperspectral Imagery Via Linear Prediction," *EEE Signal Processing Letters*, vol. 12, no. 2, pp. 138–141, Jan. 2005.

[16] S.-C. Tai, T.-M. Kuo, C.-H. Ho, and T.-W. Liao, "A Near-lossless Compression Method Based on CCSDS for Satellite Images," *International Symposium on Computer, Consumer and Control*, Jun. 2012.

[17] D. Valsesia and E. Magli, "A Novel Rate Control Algorithm for Onboard Predictive Coding of Multispectral and Hyperspectral Images," *IEEE Transactions on Geoscience and Remote Sensing*, vol. 52, no. 10, pp. 6341–6355, Jan. 2014.

[18] M. Conoscenti, R. Coppola, and E. Magli, "Constant SNR, Rate Control, and Entropy Coding for Predictive Lossy Hyperspectral Image Compression," *IEEE Transactions on Geoscience and Remote Sensing*, vol. 54, no. 12, pp. 7431–7441, Dec. 2016.

[19] D. Valsesia and E. Magli, "Fast and Lightweight Rate Control for Onboard Predictive Coding of Hyperspectral Images," *IEEE Geoscience and Remote Sensing Letters*, vol. 14, no. 3, pp. 394–398, Mar. 2017.

[20] J. Bartrina-Rapesta, I. Blanes, F. Auli-Llinas, J. Serra-Sagrista, V. Sanchez, and M. W. Marcellin, "A Lightweight Contextual Arithmetic Coder for On-Board Remote Sensing Data Compression," *IEEE Transactions on Geoscience and Remote Sensing*, vol. 55, no. 8, pp. 4825–4835, Aug. 2017.

[21] Consultative Committee for Space Data Systems (CCSDS). [Online]. Available: http://www.ccsds.org

[22] *Lossless Multispectral & Hyperspectral Image Compression*, CCSDS-123.0-B-2 Blue Book, Feb. 2019.

[23] J. Bartrina-Rapesta, M. W. Marcellin, J. Serra-Sagrista, and M. Hernandez-Cabronero, "A Novel Rate-Control for Predictive Image Coding With Constant Quality," *IEEE Access*, vol. 7, pp. 103 918–103 930, Jul. 2019.

[24] E. Auge, J. E. Sanchez, A. Kiely, I. Blanes, and J. Serra-Sagrista, "Performance Impact of Parameter Tuning on the CCSDS-123 Lossless Multi- and Hyperspectral Image Compression Standard," *Journal of Applied Remote Sensing*, vol. 7, no. 1, pp. 074 594–074 594, Aug. 2013.